Nonlinear Transient Growth and Boundary Layer Transition

Pedro Paredes,* Meelan M. Choudhari,† and Fei Li‡
NASA Langley Research Center, Hampton, VA 23681

Parabolized stability equations (PSE) are used in a variational approach to study the optimal, non-modal disturbance growth in a Mach 3 flat plate boundary layer and a Mach 6 circular cone boundary layer. As noted in previous works, the optimal initial disturbances correspond to steady counter-rotating streamwise vortices, which subsequently lead to the formation of streamwise-elongated structures, i.e., streaks, via a lift-up effect. The nonlinear evolution of the linearly optimal stationary perturbations is computed using the nonlinear plane-marching PSE for stationary perturbations. A fully implicit marching technique is used to facilitate the computation of nonlinear streaks with large amplitudes. To assess the effect of the finite-amplitude streaks on transition, the linear form of plane-marching PSE is used to investigate the instability of the boundary layer flow modified by spanwise periodic streaks. The onset of bypass transition is estimated by using an N-factor criterion based on the amplification of the streak instabilities. Results show that, for both flow configurations of interest, streaks of sufficiently large amplitude can lead to significantly earlier onset of transition than that in an unperturbed boundary layer without any streaks.

Nomenclature

G	energy gain
M	Mach number
$\mathbf{M}$	energy weight matrix
(x, y, z)	Cartesian coordinates
(ξ, η, ζ)	streamwise, wall-normal and spanwise coordinates
h_1	streamwise metric factor
h_3	spanwise metric factor
ρ	density
ν	kinematic viscosity
(u, v, w)	streamwise, wall-normal and spanwise velocity components
T	temperature
$\bar{\mathbf{q}}$	vector of base flow variables
$\tilde{\mathbf{q}}$	vector of perturbation variables
$\hat{\mathbf{q}}$	vector of amplitude variables
T_w	wall temperature
T_{ad}	adiabatic wall temperature
Re	Reynolds number
α	streamwise wavenumber
β	spanwise wavenumber
m	azimuthal wavenumber
L	flat plate characteristic length
δ	boundary layer thickness
ω	angular frequency

*NASA NPP Fellow, Computational AeroSciences Branch. AIAA Member
†Research Scientist, Computational AeroSciences Branch. AIAA Associate Fellow
‡Research Scientist, Computational AeroSciences Branch.

J	objective function
E	energy norm
N_E	logarithmic amplification factor based on energy norm
Ω	domain of integration
$\mathcal{K}$	bilinear concomitant
$\mathcal{L}$	Lagrangian function
$\mathbf{A}$, $\mathbf{B}$, $\mathbf{C}$, $\mathbf{D}$, $\mathbf{L}$, $\mathbf{P}$, $\mathbf{Q}$	linear matrix operators

Subscript

r	reference value
0	initial position
1	final position

Superscripts

$*$	dimensional value
$\dagger$	adjoint
T	transpose
H	conjugate transpose

Abbreviations

EVP	EigenValue Problem
FM_1	First Mode with fundamental wavelength
$FM_{1/2}$	First Mode with subharmonic wavelength
LST	Linear Stability Theory
NS	Navier-Stokes
OSE	Orr-Sommerfeld and Squire Equations
PDE	Partial Differential Equations
PSE	Parabolized Stability Equations
S	Sinuous secondary instability
SS	Subharmonic Sinuous secondary instability
SV	Subharmonic Varicose secondary instability
V	Varicose secondary instability

I. Introduction

The most common approach to transition prediction relies on exponential or modal amplification of discrete modes. The classic linear stability theory is mainly concerned with individual sinusoidal waves propagating in the boundary layer parallel to the wall. In this context, the quasi-parallel flow approximation is typically used, and the linearized equations of fluid motion lead to an eigenvalue problem, which may be expressed in the limit of incompressible flows in the form of the Orr-Sommerfeld and Squire equations (OSE).[1,2] Effects of weak non-parallelism in mean-flow can be accounted for by using multiple scale theory, which yields the leading order correction to the local amplification rate and phase speed predicted by the quasi-parallel theory. A more useful extension to the non-parallel stability theory was proposed by Herbert,[3] who introduced the concept of Parabolized Stability Equations (PSE). Since then, the PSE technique has been applied to a variety of problems, including linear and nonlinear evolution of instability waves in 2D and 3D shear flows across a broad range of speeds.

Besides the exponential growth characteristics of convectively unstable eigenmodes in a boundary layer flow, the external disturbances, e.g., freestream turbulence and surface roughness, can also have a large influence on the transition process. An additional route to transition may involve nonmodal growth, which refers to situations in which transient growth of disturbance energy is observed even when the flow is modally stable, i.e., all eigenmodes are damped. Mathematically, the transient growth is associated with the non-orthogonality of the eigenvectors corresponding to the linear disturbance equations. Physically, the main growth mechanism corresponds to the lift-up effect, which results from the conservation of horizontal momentum when the fluid particles are displaced vertically, i.e., along the wall-normal direction.

The nonmodal, or equivalently transient, growth mechanism has been extensively studied in a large variety

of flows. The algebraic inviscid lift-up instability mechanism was originally identified by Stuart,[4] Ellingsen & Palm,[5] and Landahl[6] for inviscid shear flows. In the 1990s, numerous temporal nonmodal growth studies of incompressible two-dimensional shear flows assuming a parallel-flow approximation appeared, among others by Butler & Farrel,[7] Reddy & Henningson[8] and Trefethen et al.[9] Lately, Hanifi et al.[10] included the compressibility effects in their study of temporal, nonmodal transient growth in zero-pressure-gradient flat plate boundary layers. The first spatial analysis of nonmodal growth in a Blasius boundary layer was presented by Andersson et al.[11] and Luchini,[12] who used the linearized boundary region equations. The latter equations include the nonparallel effects associated with boundary layer development that were missing from the temporal formulations of transient growth. The nonmodal analysis of compressible boundary layers was continued by Tumin & Reshotko,[13] who reformulated the temporal analysis of Hanifi et al.[10] in a spatial framework, but still assuming the parallel flow approximation. The nonparallel effects were included in their subsequent publications[14–17] by solving a parabolic set of equations based on the boundary region approximation. These authors also addressed the effects of convex surface curvature by studying optimal growth in the boundary layer over a sphere.[15,16] Their findings indicated that increasing convex curvature reduces nonmodal growth. These studies also considered the effects of wall cooling and concluded that reducing the wall temperature leads to stronger nonmodal growth. Transient growth in flat plate boundary layers at hypersonic Mach numbers up to Mach 10 has been studied by Paredes et al.[18,19] Their results showed that the same physical mechanism of nonmodal growth, i.e., the conversion of streamwise vorticity into streamwise streaks via the lift-up effect, persists even at hypersonic flow conditions. The studies by Paredes et al.[18,19] also addressed the effects of viscous-inviscid interaction near the leading edge including the weak shock wave resulting from the displacement effect of the boundary layer. By comparing the transient growth magnitudes based on Navier-Stokes (NS) mean flow solutions and the self-similar approximation based on boundary layer equations, they showed that using the exact (numerical) solution leads to strong reduction of the optimal energy gain for initial disturbance locations that are sufficiently close to the plate leading edge.

Recently, transient growth has been identified as a candidate mechanism for many examples of bypass transition.[20] This term has historically been used to differentiate the well known paths to transition[21] via modal growth of hydrodynamic instabilities from transition phenomena that are not fully understood on a theoretical basis. Examples of transition often classified as bypass transition are the subcritical transition observed in Poiseuille pipe flow experiments,[22,23] transition due to distributed surface roughness on flat plates[24,25] or cones,[26] and subcritical transition observed in spherical forebodies.[27–30]

The focus of this paper is on nonlinear transient growth and boundary layer transition in high-speed flows. While the possibility of strong linear transient growth in these flows has been demonstrated,[16–19] its relation to boundary layer transition cannot be established within the framework of linear disturbances. This paper begins to address that limitation by investigating the nonlinear evolution of linearly optimal disturbances when they are initiated with finite amplitudes, and on the subsequent streak instability that is likely to result in the onset of bypass transition. Section II briefly describes the optimal growth theory based on PSE and introduces the linear plane-marching PSE for monitoring linear and nonlinear development of disturbances in three-dimensional flows with a single slowly-varying spatial direction, such as those of interest in this paper. Section III.A presents the nonlinear evolution of finite-amplitude, linearly optimal disturbances and the subsequent instability characteristics of the perturbed streaky flow in a supersonic, zero pressure gradient, flat plate boundary boundary layer at Mach 3. Analogous results for a Mach 6 flow over a sharp, 7° half-angle cone are described in Section III.B. Conclusions are presented in Section IV.

II. Methodology

This section introduces the methodologies used in this paper. First, the linear optimal growth theory based on the PSE is briefly described. This method is used to obtain the optimal initial perturbation that results in maximum energy gain at a specified downstream position. The linearly optimal perturbation with a given finite amplitude is used as the initial condition for the parabolic integration of the stationary, nonlinear plane-marching PSE to obtain a three-dimensional, spanwise-periodic, perturbed boundary layer flow. Then, the two-dimensional partial differential equation (PDE) based EVP and the linear form of the plane-marching PSE are used to study the instability characteristics of the perturbed, streaky boundary layer flows. For more details about these methodologies, as well as about the numerical discretization and boundary conditions used in this paper, see Paredes et al.[18,19,31,32]

II.A. Linear Optimal Growth using PSE

Transient growth analysis is performed using the linear PSE as explained in the literature.[19,33–35] The method is outlined here for completeness purposes. There are strong similarities with the optimization approach based on the linearized boundary layer equations.[11,12,14] The advantage of the PSE-based formulation is that it is also applicable to more complex base flows where the flow evolves slowly along the streamwise direction but the boundary layer approximation may not hold and that it can be easily extended to unsteady disturbances. While infinite Reynolds number asymptotic results cannot be directly computed using this technique, good agreement is achieved between the two methodologies for incompressible and compressible regimes as shown by Paredes et al.[18,19]

In the PSE context, the perturbations have the form

$$\tilde{\mathbf{q}}(\xi,\eta,\zeta,t) = \hat{\mathbf{q}}(\xi,\eta)\exp\left[\mathrm{i}\left(\int_{\xi_0}^{\xi}\alpha(\xi')\,\mathrm{d}\xi' + \beta\zeta - \omega t\right)\right] + \text{c.c.}, \tag{1}$$

where c.c. denotes complex conjugate. The suitably nondimensionalized, orthogonal, curvilinear coordinate system (ξ,η,ζ) denotes streamwise, wall-normal, and spanwise coordinates and (u,v,w) represent the corresponding velocity components. Density and temperature are denoted by ρ and T. The Cartesian coordinates are represented by (x,y,z). The vector of perturbation fluid variables is $\tilde{\mathbf{q}}(\xi,\eta,\zeta,t) = (\tilde{\rho},\tilde{u},\tilde{v},\tilde{w},\tilde{T})^T$ and the vector of amplitude functions is $\hat{\mathbf{q}}(\xi,\eta) = (\hat{\rho},\hat{u},\hat{v},\hat{w},\hat{T})^T$. The vector of basic state variables is $\bar{\mathbf{q}}(\xi,\eta) = (\bar{\rho},\bar{u},\bar{v},\bar{w},\bar{T})^T$. The streamwise and spanwise wavenumbers are α and β, respectively; and ω is the angular frequency of the perturbation.

Upon introduction of the perturbation form (1) into the linearized NS equations together with the assumption of a slow streamwise dependence of the basic state and the amplitude functions, thus neglecting the viscous derivatives in ξ, the PSE are recovered as follows

$$\left(\mathbf{A} + \mathbf{B}\frac{\partial}{\partial\eta} + \mathbf{C}\frac{\partial^2}{\partial\eta^2} + \mathbf{D}\frac{1}{h_1}\frac{\partial}{\partial\xi}\right)\hat{\mathbf{q}}(\xi,\eta) = 0. \tag{2}$$

The linear operators $\mathbf{A}$, $\mathbf{B}$, $\mathbf{C}$ and $\mathbf{D}$ are given by Pralits et al.[33] and h_1 is the metric factor associated with the streamwise curvature. The system of Eqs. (2) is not fully parabolic due to the term $\partial\hat{p}/\partial\xi$ in the streamwise momentum equation.[36–40] However, for the purely stationary disturbances of interest in this work, this term can be dropped from the equations as justified by Refs. [34, 41], who found that the term, $\partial\hat{p}/\partial\xi$, is of higher order for transient growth problems, and can be neglected without any loss of accuracy.

The optimal initial disturbance, $\tilde{\mathbf{q}}_0$, is defined as the initial (i.e., inflow) condition at ξ_0 that experiences the maximum energy amplification up to a specified position, ξ_1. Thus, the following objective function needs to be maximized,

$$J(\tilde{\mathbf{q}}) = \frac{E(\xi_1)}{E(\xi_0)}, \tag{3}$$

where E denotes the energy norm of $\tilde{\mathbf{q}}$,

$$E(\xi) = \int_\zeta\int_\eta \tilde{\mathbf{q}}(\xi,\eta,\zeta)^H\mathbf{M}\tilde{\mathbf{q}}(\xi,\eta,\zeta)\,h_1\,h_3\,\mathrm{d}\eta\,\mathrm{d}\zeta, \tag{4}$$

where h_3 is the metric factor associated with the azimuthal curvature, $\mathbf{M}$ is the energy weight matrix and the superscript H denotes conjugate transpose. In the present case, the spanwise direction is homogeneous, i.e., the basic state is independent of the spanwise coordinate and the perturbations are periodic along this coordinate. Therefore, instead of the definition of Eq. (4), the following one dimensional definition is used for the solution of the linear optimization,

$$E(\xi)_\eta = \int_\eta \hat{\mathbf{q}}(\xi,\eta)^H\mathbf{M}\hat{\mathbf{q}}(\xi,\eta)\,h_1\,h_3\,\mathrm{d}\eta = \frac{1}{2}E(\xi). \tag{5}$$

Nevertheless, both definitions are related by a constant value of 2, so the linear optimization solution is invariant of this selection; and in what follows, the two-dimensional definition of Eq. (4) will be used for consistency with the nonlinear part of the paper. Furthermore, the following spanwise-independent definition of the energy is also used to compare energy of disturbances with different spanwise wavenumbers,

$$\hat{E}(\xi) = \frac{1}{L_\zeta}\int_{\zeta-L_\zeta/2}^{\zeta+L_\zeta/2} E(\xi)_\eta\,\mathrm{d}\zeta = \frac{2}{L_\zeta}E(\xi)_\eta = \frac{1}{L_\zeta}E(\xi) \tag{6}$$

where $L_\zeta = 2\pi/\beta$ is the spanwise wavelength.

The choice of the energy norm would have an effect on the results. Here, the general approximation followed by Tempelmann et al.[35] is used, which is based on all five state variables. This formulation uses the positive-definite energy norm derived by Mack[42] and Hanifi et al.,[10] which is defined by

$$\mathbf{M} = \mathrm{diag}\left[\frac{\bar{T}(\xi,\eta)}{\gamma\bar{\rho}(\xi,\eta)M^2}, \bar{\rho}(\xi,\eta), \bar{\rho}(\xi,\eta), \bar{\rho}(\xi,\eta), \frac{\bar{\rho}(\xi,\eta)}{\gamma(\gamma-1)\bar{T}(\xi,\eta)M^2}\right]. \tag{7}$$

The variational formulation[19] leads to an optimality system, which is solved in an iterative manner, starting from a random solution at ξ_0, which must satisfy the boundary conditions. The PSE, $\mathbf{L}\tilde{\mathbf{q}} = 0$, are used to integrate $\tilde{\mathbf{q}}$ up to ξ_1, where the final optimality condition is used to obtain the initial condition for the backward adjoint PSE integration, $\mathbf{L}^\dagger\tilde{\mathbf{q}}^\dagger = 0$. At ξ_0, the adjoint solution is used to calculate the new initial condition for the forward PSE integration with the initial optimality condition. The iterative procedure finishes when the objective function, $J = G = E_1/E_0$ is converged up to a certain tolerance, which was set to 10^{-4} in the present computations.

II.B. Plane-Marching PSE

The plane-marching PSE technique extends the classical line-marching PSE for base flows with a single strongly inhomogeneous direction to base flows with a mild variation in the streamwise coordinate and strong gradients in the other two spatial directions, i.e., the wall-normal and spanwise directions in boundary layer problems. Similar to the derivation of the classical PSE, the disturbance quantities are expanded in terms of their truncated Fourier components assuming that they are periodic in time as

$$\tilde{\mathbf{q}}(\xi,\eta,\zeta,t) = \sum_{n=-N}^{N} \hat{\mathbf{q}}_n(\xi,\eta,\zeta)\exp\left[\mathrm{i}\left(\int_{\xi_0}^{\xi}\alpha_n(\xi')\,\mathrm{d}\xi' - n\omega t\right)\right] + \mathrm{c.c.} \tag{8}$$

Substituting Eq. (8) into the NS equations and neglecting the viscous derivatives in ξ, the nonlinear plane-marching PSE can be written in a compact form as

$$\left(\mathbf{P}_n + \mathbf{Q}_n\frac{\partial}{\partial\eta} + \mathbf{R}_n\frac{\partial^2}{\partial\eta^2} + \mathbf{S}_n\frac{1}{h_3}\frac{\partial}{\partial\zeta} + \mathbf{T}_n\frac{1}{h_3^2}\frac{\partial^2}{\partial\zeta^2} + \mathbf{V}_n\frac{1}{h_1}\frac{\partial}{\partial\xi}\right)\hat{\mathbf{q}}_n(\xi,\eta,\zeta) = \mathbf{F}_n(\xi,\eta,\zeta)\exp\left(\mathrm{i}\int_{\xi_0}^{\xi}\alpha_n(\xi')\,\mathrm{d}\xi'\right), \tag{9}$$

where $\mathbf{F}_n$ is the Fourier component of the total forcing $\mathbf{F}$ that contains the nonlinear terms. The entries of the coefficient matrices for $\mathbf{P}_n$ $\mathbf{Q}_n$, $\mathbf{R}_n$, $\mathbf{S}_n$, $\mathbf{T}_n$, $\mathbf{V}_n$ and vector $\mathbf{F}$ are found in Paredes.[43]

In this work, the nonlinear formulation of the plane-marching PSE[44] is used to follow the development of finite-amplitude optimal disturbances (i.e., streaks). A fully implicit formulation has been adopted to facilitate the convergence of the solution for high streak amplitudes. For the stationary disturbances of interest in this paper, $N = 0$ and $\alpha_0 = 0$.

The linear form of the plane-marching PSE, which are recovered from Eq. (9) by setting $\mathbf{F} = 0$, are also used herein to study the linear stability characteristics of the modified basic state corresponding to the sum of the unperturbed boundary layer and the finite-amplitude optimal disturbance. The perturbed boundary layer flow with streaks is characterized by local regions of high gradient in streamwise velocity distribution across the streak, which can sustain the growth of shear-layer instability modes. The advantage of using the plane-marching PSE with respect to the PDE-based two-dimensional EVP is that the plane-marching PSE account for the non-parallel development of the flow. Nevertheless, the solution of the PDE-based EVP provides a convenient means to obtain the shape function, wavenumber, and damping/growth-rate, required as initial conditions for the plane-marching PSE integration.

III. Results

A flat plate boundary layer flow at freestream Mach number of 3 with adiabatic wall and a 7° half-angle circular cone boundary layer flow at freestream Mach number of 6 with isothermal wall are studied next. The selected flow conditions are representative of the instability characteristics of two-dimensional and axisymmetric boundary layers in the supersonic and hypersonic regimes. Furthermore, the above choice of flow conditions allows us to build upon the previous analyses of linear optimal growth in Refs. [18, 19].

III.A. Mach 3 Flat Plate Boundary Layer

The first flow configuration of interest corresponds to a supersonic, flat plate boundary layer with $M = 3$, $T_0 = 333\,\mathrm{K}$, and an adiabatic wall. Only a summary of the results obtained for this case is presented here. For a comprehensive discussion of the findings, the reader is referred to Ref. [31]. For this problem, the computational and Cartesian coordinates coincide, i.e., $(\xi, \eta, \zeta) \equiv (x, y, z)$. The self-similar scale proportional to boundary layer thickness is $\delta = \sqrt{x^* \nu_r^* / u_r^*} = x^*/\sqrt{Re_\delta}$, where subscript r denotes reference values and the superscript $*$ indicates dimensional values. The PSE are nondimensionalized with δ_1, i.e., the value of δ at the final location corresponding to $x_1^* = L$, where L denotes a reference body length scale. Therefore, the Reynolds number introduced into the equations becomes $Re_{\delta_1} = \sqrt{Re_L}$. In what follows and in line with the literature, x^* is scaled by L, while the remaining two spatial variables are nondimensionalized with δ_1. The streamwise location is written as $R = Re_\delta = \sqrt{x^* u_r^* / \nu_r^*}$.

The instability of the unperturbed, adiabatic, Mach 3 flat-plate boundary layer flow is examined by PSE to establish the transition behavior in the absence of stationary streak perturbations. The onset of laminar-turbulent transition is estimated using the logarithmic amplification ratio based on the energy norm E of Eq. (7),

$$N_E = -\int_{\xi_{lb}}^{\xi} \alpha_i(\xi')\, d\xi' + 1/2 \log\left[\hat{E}(\xi)/\hat{E}(\xi_{lb})\right], \tag{10}$$

relative to the location ξ_{lb} where the disturbance first becomes unstable. The N-factor evolution of the oblique first modes is computed with the PSE. Accordingly, we assume that transition onset is likely to occur when the peak N-factor reaches a specified value. Figure 1(b) shows the N-factor curves based on the energy norm E of Eq. (7) of first modes with spanwise wavenumbers from $\beta = 0.025$ to 0.135 and frequencies from $\omega = 0.006$ to 0.046. The first modes that reach $N_E = 5$ and $N_E = 10$ are chosen as representative threshold values for laminar-turbulent transition under noisy or quiet conditions, respectively. Calculations show that $N_E = 5$ is reached at $R = 1,596$ (i.e., $Re_x = 2.55 \times 10^6$) and $N_E = 10$ is achieved at $R = 3,226$ ($Re_x = 1.04 \times 10^7$).

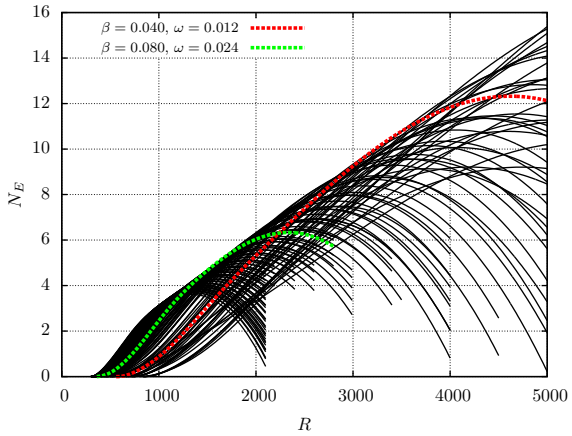

Figure 1. PSE predictions for N-factor based on energy norm E of oblique first mode disturbances in an unperturbed Mach 3 boundary layer with adiabatic wall. The spanwise wavenumber is varied from $\beta = 0.025$ to 0.135 and the frequency from $\omega = 0.006$ to 0.046. The thick lines denote the spanwise wavenumber and frequency combination that first reaches (green) $N_E = 5$ ($\beta = 0.080$, $\omega = 0.024$) and (red) $N_E = 10$ ($\beta = 0.040$, $\omega = 0.012$).

As described in Refs. [18, 19], the basic state is obtained from a numerical solution of the NS equations, which account for both the viscous-inviscid interaction near the leading edge and the weak shock wave emanating from that region. The leading edge radius is set to $r_n = 1$ μm and the freestream unit Reynolds number to $Re' = 10^6/\mathrm{m}$. The effects of the viscous-inviscid interaction and the shock wave translate into a deviation from the self-similar solution, as noted by Paredes et al.[18,19] The streamwise velocity and temperature profiles converge to the self-similar solution with $R > 100$. These effects produce a maximum 9% deviation from transient growth results based on self-similar base flow when the initial optimization position is located near the leading edge.

Transient growth results corresponding to the basic state obtained from NS equations is shown in Figure 2(a) for $R_1 = 1,000$ with $x_1 = L = 1$ m as the final optimization position. The initial location that leads to maximum energy gain up to $R_1 = 1,000$ corresponds to $R_0 = 500$ ($x_0 = 0.25$).[18,19] As shown in Fig. 2(a),

the maximum gain occurs at a spanwise wavenumber of $\beta = 0.3$. The optimal initial perturbation, $\hat{\mathbf{q}}_0$, and the perturbation at the final optimization location, $\hat{\mathbf{q}}_1$, for the above wavenumber are shown in Figs. 2(b) and 2(c), respectively.

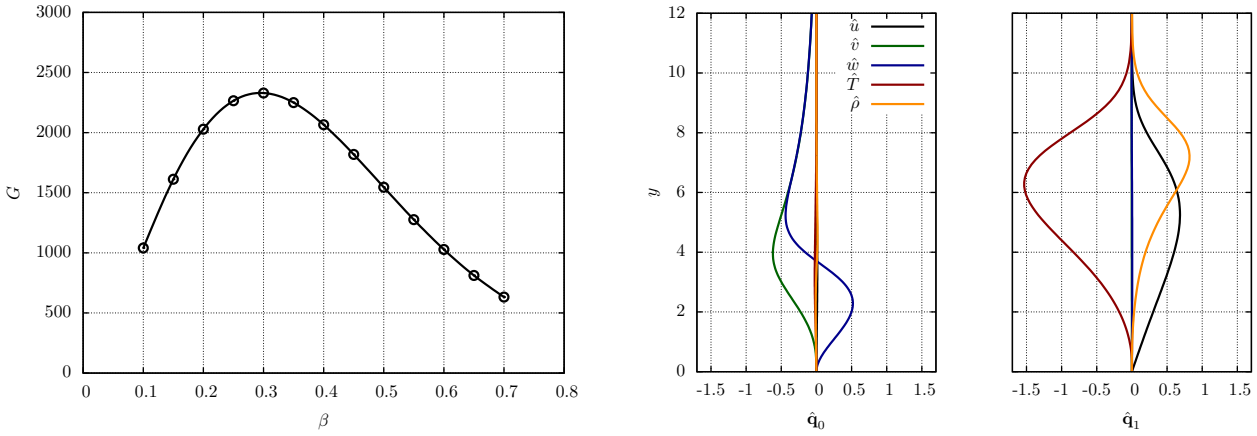

(a) Optimum energy gain (b) Initial perturbation (c) Final perturbation

Figure 2. Optimal energy gain in the adiabatic, Mach 3 flat plate boundary layer with initial and final disturbance locations at $R_0 = 500$ and $R_1 = 1,000$, respectively. Also, initial and final amplitude vectors with $\beta = 0.3$. The amplitude vectors are normalized with local energy norm $\hat{E}$ as defined in Eq. (6).

The nonlinear form of the plane-marching PSE is used to monitor the nonlinear development of the initial disturbance from Fig. 2(b). Figure 3(a) shows the evolution of the streak amplitude based on u,

$$As_u(\xi) = [\max_{\eta,\zeta}(\tilde{u}(\xi,\eta,\zeta)) - \min_{\eta,\zeta}(\tilde{u}(\xi,\eta,\zeta))]/2, \tag{11}$$

for selected amplitudes of the optimal inflow perturbation. Unlike the energy norm in Eq. (4), the velocity amplitude As_u can be measured in wind tunnel experiments (at least up to moderately high Mach numbers). It is also expected to have a more direct connotation for the growth of streak instability. The streak amplitude parameter A corresponds to the maximum streak amplitude As_u achieved by a linear perturbation with the same initial amplitude, which is given by

$$A_0 = A \times \sqrt{E_{lin,A=1}}, \tag{12}$$

with $E_{lin,A=1} = 1.79 \times 10^{-2}$. As indicated by Eq. (12), the amplitude parameter A provides a convenient measure of the initial disturbance amplitude. As seen in Fig. 3(a), the nonlinear effects reduce the streak amplitude relative to the linear prediction; and hence, for any given case, $\max(As_u) < A$. This maximum moves progressively upstream as the amplitude parameter A is increased. In the incompressible case, a similar trend was observed by Andersson et al.[45] with direct numerical simulations and by Martin & Martel[46] with boundary region equations. Figures 3(b) and 3(c) show the streamwise evolution of the massflux contours for the $A = 0.41$ and $A = 1.38$ streaks, respectively. At the symmetry plane, $z = L_z/2$, the near-wall, low-momentum fluid is lifted upward by the counter-rotating vortices, resulting in a localized region of large boundary layer thickness and lower wall shear, $\tau_w = \mu(\partial u/\partial y)_w$, where the subscript w refers to the wall location ($y_w = 0$). At the lateral symmetry plane, $z = 0$ (and $z = L_z$), the effect of the initial streamwise vortices is exactly the opposite, yielding a localized region of reduced boundary layer thickness and increased wall shear. A comparison of Figs. 3(b) for $A = 3$ and 3(c) for $A = 10$, shows that the higher streak amplitude leads to a more complex flow pattern in the form of a mushroom-like flow structure.

To assess the effect of the nonlinear stationary disturbances on transition, the PDE-based EVP analysis is used in conjunction with the linear form of the plane-marching PSE to investigate the instability of the Mach 3 flat plate boundary layer flow modified by spanwise periodic streaks. The PDE-based EVP analysis is used to obtain the growth rates of fundamental and subharmonic sinuous and varicose modes at $R = 1,000$ for the streaks shown in Figure 3(a). These instabilities are supported by the detached three-dimensional shear-layer formed by the streaks. Results for the instability modes corresponding to the fundamental spanwise wavenumber, i.e., equal to the spanwise wavenumber of the streak, and subharmonic instability modes with double spanwise wavelength, i.e., half spanwise wavenumber, are shown in Fig. 4 for the streaks initiated at $R_0 = 500$ with a spanwise wavenumber of $\beta = 0.30$. Local growth rates at $R = 1,000$ are plotted as a

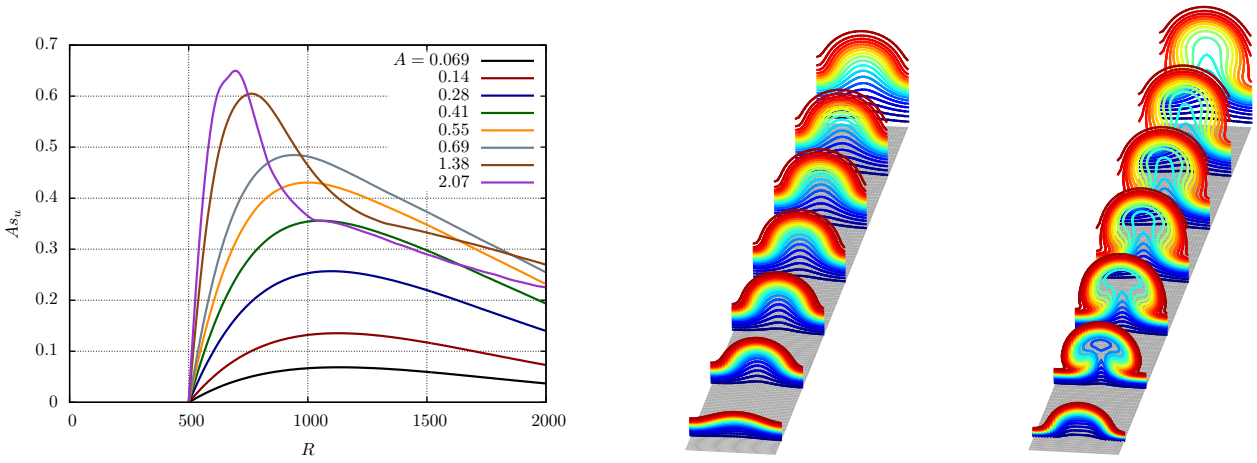

(a) Evolution of streaks amplitude, As_u (b) $\bar{\rho}\bar{u}$, $A = 0.41$ (c) $\bar{\rho}\bar{u}$, $A = 1.38$

Figure 3. (a) Evolution of streak amplitudes based on u, As_u, of finite-amplitude streaks initialized at the optimal initial position, $R_0 = 500$, with $\beta = 0.30$. (b,c) Isolines of streamwise massflux, $\bar{\rho}\bar{u}$, for the $A = 0.41$ and $A = 1.38$ streaks.

function of disturbance frequency in Fig. 4. For reference, the growth rates of the first mode instabilities for the unperturbed flow ($A = 0$), corresponding to the same wavenumber as the streak (FM_1), i.e., $\beta = 0.3$, and to one half of the streak wavenumber ($\mathrm{FM}_{1/2}$), i.e., $\beta = 0.15$, are also included in Figs. 4(a) and 4(b), respectively. For the spanwise wavenumber of $\beta = 0.3$, the first mode is stable at $R = 1,000$, but for the subharmonic case, the first mode with $\beta = 0.15$ is unstable at $R = 1,000$. A thorough study of the interaction of low to moderate amplitude streaks with the oblique first mode instability is presented by Paredes et al.[47] As previously observed in the incompressible regime,[45] the sinuous (S) mode is found to become unstable at lower streak amplitudes than those required for the onset of the varicose (V) mode. Specifically, the threshold streak amplitude for the S mode is found to be approximately $As_u \approx 0.2$. The threshold amplitude for the V mode is significantly higher, equal to $As_u \approx 0.35$. Figure 4(b) indicates that, similar to the fundamental wavelength modes in Fig. 4(a), the growth rates of subharmonic modes increase with the streak amplitude and the subharmonic sinuous (SS) modes are more unstable than the subharmonic varicose (SV) modes. The SS mode converges to the $\mathrm{FM}_{1/2}$ mode as A is decreased. Therefore, there is no streak amplitude threshold for SS modes. While the peak growth rates of the SS modes are lower than their fundamental counterparts, the SV modes have slightly larger growth rates than the corresponding fundamental modes. Of course, because of the complex dependence of the secondary growth rate on the structure of the streak, one must investigate the overall amplification of the various disturbance modes in order to assess their relative roles during the transition process. Results on this type are presented later in this section.

The magnitude of the streamwise velocity shape functions, $|\hat{u}|$, for the S and V modes are plotted in Fig. 5 for the streamwise location of $R = 1,000$. The SS and SV mode shapes in Fig. 6 are very similar to the mode shapes of corresponding fundamental modes in Fig. 5. However, the relative phase distributions associated with the fundamental and subharmonic modes are rather different. Whereas the phase distributions within adjacent streaks are identical to each other in the case of fundamental modes, those of the subharmonic modes are antisymmetric, i.e., correspond to mirror images of each other; see Paredes et al.[31] for more details. The close alignment between the locations of peak instability fluctuations and the critical layer surface indicates that these instability modes are related to the instability of the three-dimensional shear layer.

Next, we examine the spatial evolution of fixed frequency secondary disturbances in terms of the N-factor definition of Eq. 10. N-factor curves for sinuous modes (S and SS) at selected frequencies are plotted in Fig. 7. The predictions for S modes are plotted in Fig. 7(a), whereas those corresponding to SS modes are shown in Fig. 7(b). Over the range of frequencies plotted in Figs. 7(a) and 7(b), the SS modes become unstable at a farther upstream station. More important is the fact that the SS modes that first achieve N-factors of between 5 and 14 are expected to correlate to the onset of transition in a broad range of disturbance environments. The S modes first become unstable at a streamwise position that is downstream of the streak initialization at $R_0 = 500$. On the other hand, the SS modes originate upstream of $R_0 = 500$ as first mode instabilities of the unperturbed boundary layer and then morph into the shear layer modes as the streak

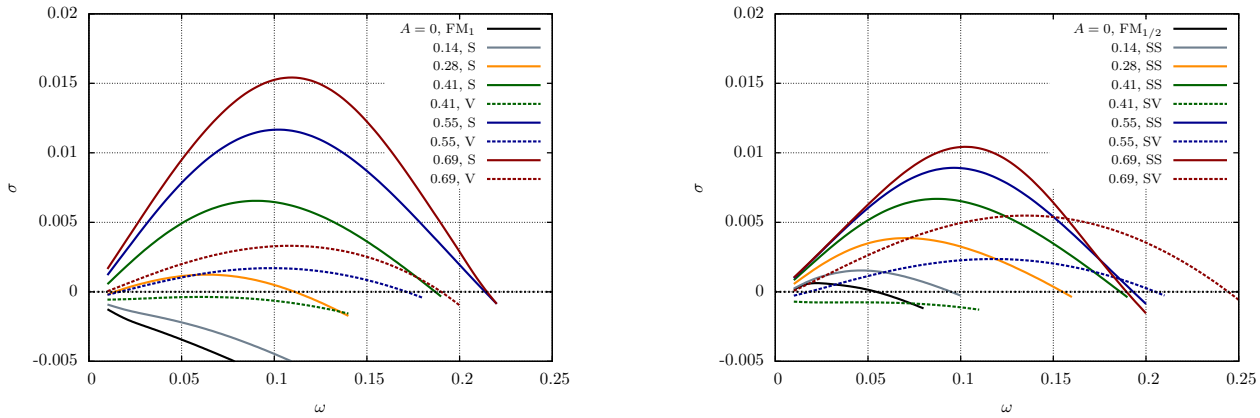

(a) Growth rate of fundamental streak instability modes

(b) Growth rate of subharmonic streak instability modes

Figure 4. Growth rates ($\sigma = -\alpha_i$) of (a) fundamental sinuous (S) and varicose (V) modes and (b) subharmonic sinuous (SS) and subharmonic varicose (SV) modes of finite-amplitude streaks initialized at the optimal initial position, $R_0 = 500$, with $\beta = 0.30$, computed with PDE-based EVP. The analysis is performed at location $R = 1,000$.

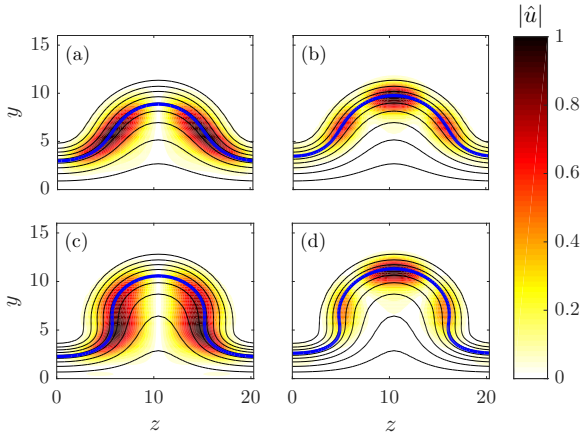

Figure 5. Isocontours of the modulus of streamwise velocity fluctuations associated with the (a,c) S and (b,d) V modes of the streaks with (a,b) amplitude $A = 0.41$ and frequency $\omega = 0.09$ and (c,d) amplitude $A = 0.69$ and frequency $\omega = 0.11$. The isolines of basic state mass flux $\bar{\rho}\bar{u} = 0.1 : 0.1 : 0.9$ are included. Also, the critical layer, $\bar{u} = c_{ph}$, where $c_{ph} = \omega/\alpha_r$ is the phase speed of the instability wave, is added for reference with thick solid blue lines.

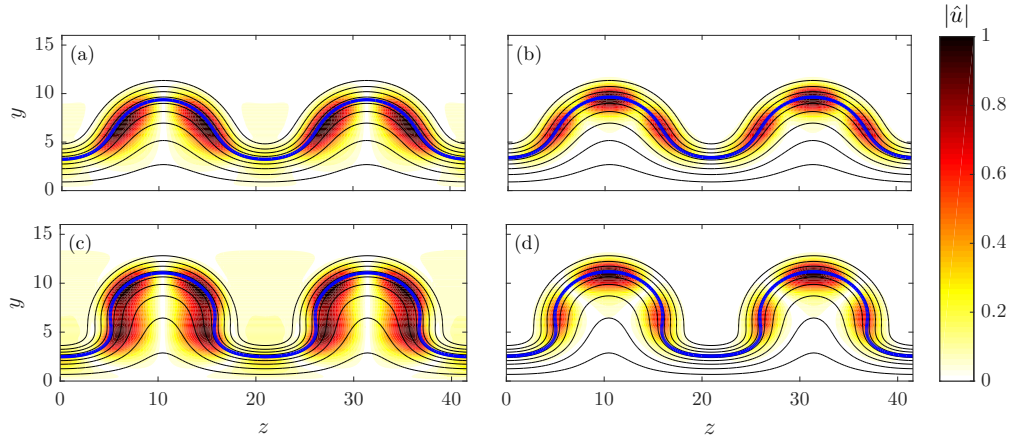

Figure 6. Isocontours of the modulus of streamwise velocity fluctuations associated with the (a,c) SS and (b,d) SV modes of the streaks with (a,b) amplitude $A = 0.41$ and frequency $\omega = 0.09$ and (c,d) amplitude $A = 0.61$ and frequency $\omega = 0.10$. The isolines of basic state mass flux $\bar{\rho}\bar{u} = 0.1 : 0.1 : 0.9$ are included. Also, the critical layer, $\bar{u} = c_{ph}$, where $c_{ph} = \omega/\alpha_r$ is the phase speed of the instability wave, is added for reference with thick solid blue lines.

amplitude increases.

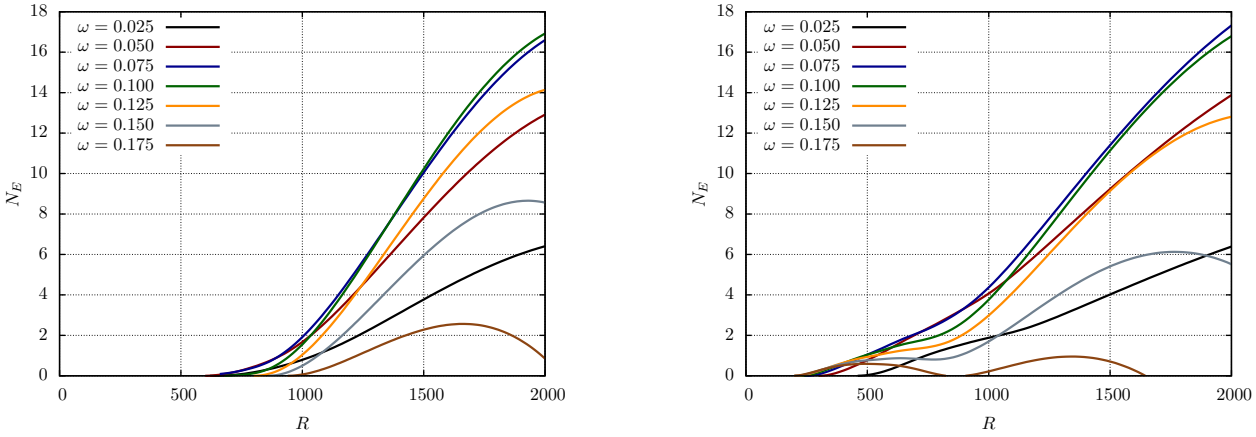

(a) N-factor of S mode

(b) N-factor of SS mode

Figure 7. N**-factors based on** E **of (a) S and (b) SS instability modes computed with plane-marching PSE for the streaks initiated at** $R_0 = 500$ **with** $\beta = 0.30$ **and streak amplitude parameter** $A = 0.41$**.**

N-factor contours in the Re_x - $\hat{E}_0$ plane corresponding to fundamental and subharmonic, sinuous, instability modes are plotted in Fig. 8. The displayed N-factor values are $N_E = 5$, 10, and 15. A minimum threshold initial streak amplitude is required to reach any N-factor value between $N_E = 5$ and $N_E = 15$. For the purpose of discussion, the N-factor curve corresponding to $N_E = 5$ may be assumed to represent the expected variation of transition onset location in a relatively noisy disturbance environment such as a conventional ground facility, whereas the curve $N_E = 10$ may be assumed to correspond to a quiet tunnel or a flight disturbance environment. All N-factor curves in Fig. 8 have a large negative slope to begin with and approach a nearly horizontal asymptote further downstream. This implies a rapid upstream movement in transition onset once a threshold streak amplitude is exceeded and, also, an approximate saturation in the transition front location after a sufficiently high streak amplitude has been reached. In a noisy environment, the initial streak amplitude required to induce bypass transition via streak instabilities corresponds to $\hat{E}_0 \approx 1.4 \times 10^{-5}$, i.e., $As_{u,max} \approx 0.13$. The corresponding streak amplitude levels for a quiet environment ($N_E = 10$) are $\hat{E}_0 \approx 5.0 \times 10^{-5}$, i.e., $As_{u,max} \approx 0.22$. Thus, regardless of the disturbance environment, a relatively narrow range of minimum streak amplitudes ($1.4 \times 10^{-5} < \hat{E}_0 < 5.0 \times 10^{-5}$) can bring about bypass transition via streak instabilities. Not surprisingly, the effect of streaks on upstream movement in transition is somewhat weaker in the case of a noisy environment, in that the asymptote corresponding to high streak amplitudes corresponds to a projected transition onset location of $x_{tr}/x_{tr(As_u=0)} \approx 0.36$, whereas large amplitude streaks in a quieter unsteady environment can advance the onset of transition as far upstream as $x_{tr}/x_{tr(As_u=0)} \approx 0.12$. Even though instabilities of streaks with an initial amplitude of $\hat{E}_0 < 1.5 \times 10^{-5}$ can reach $N_E = 5$, the spatial location where this N-factor is reached is downstream of the location where first mode instabilities in the unperturbed boundary layer reach the same N-factor. Thus, streaks with an initial amplitude of $\hat{E}_0 < 1.5 \times 10^{-5}$ are unlikely to induce transition in noisy environments. This initial streak amplitude may, therefore, be viewed as the critical value for an upstream movement in transition location in these environments.

III.B. Mach 6 Circular Cone Boundary Layer

Next, we examine the role of finite amplitude streaks in inducing bypass transition in the axisymmetric boundary layer over a 7° circular cone in Mach 6 free stream. The length of the nearly sharp cone is $L = 0.305$ m and the nose radius is $r_n = 0.126$ mm. The freestream conditions are selected to replicate those of a previous experiment in the VKI H3 hypersonic tunnel,[48] i.e., Mach 6 flow at a unit Reynolds number of 18×10^6/m, and freestream temperature of $T_r = 60.98$ K. For this problem, the computational coordinates, (ξ, η, ζ), are defined as an orthogonal body-fitted coordinate system. The metric factors are defined as

$$h_1 = 1 + \kappa\eta, \tag{13}$$

$$h_2 = 1, \tag{14}$$

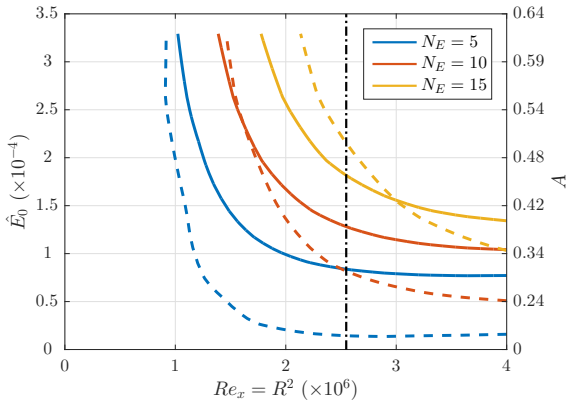

Figure 8. N**-factor based on energy norm ($N_E = 5$, 10, and 15) of fundamental (solid lines) and subharmonic (dashed lines) sinuous, secondary instability modes on a Mach 3 flat plate boundary layer perturbed by optimal streaks with initial energy of $\hat{E}_0 = 1/L_z\, E_0$ initiated at $R_0 = 500$. The vertical dot-dashed line denotes the transition location based on $N_E = 5$ (dot-dashed line) of first oblique mode in the unperturbed flow.**

$$h_3 \quad = \quad r_b + \eta\cos(\theta), \tag{15}$$

where κ denotes the streamwise curvature, r_b is the local radius, and θ is the local half-angle along the axisymmetric surface, i.e., $\sin(\theta) = dr_b/d\xi$. For the present straight circular cone (with exception of the nose region that is not included in this analysis), $\kappa \equiv 0$ and θ is the half-angle of the cone equal to 7°. Note that the spanwise wavenumber β of Eq. (1) with $1/L$ dimensions, becomes a nondimensional, integer azimuthal wavenumber, denoted by m.

Experimental measurements and theoretical predictions based on quasi-parallel, linear stability theory (LST) and the non-parallel, PSE have confirmed that laminar-turbulent transition in this flow is driven by the modal growth of planar Mack mode instabilities.[48] The instability of the unperturbed flow is examined by PSE to establish the transition behavior in the absence of stationary streak perturbations. The onset of laminar-turbulent transition in the unperturbed boundary layer flow is estimated using N-factor evolution of the planar Mack modes computed with the PSE. For the conditions of the experiment,[48] transition onset in the unperturbed cone boundary layer was measured to occur near $x/L = 0.6$. Figure 9 shows that the peak N-factor at the measured transition location corresponds to $N_E = 6$, which is reached by a planar Mack mode disturbance with frequency $F = 550$ kHz.

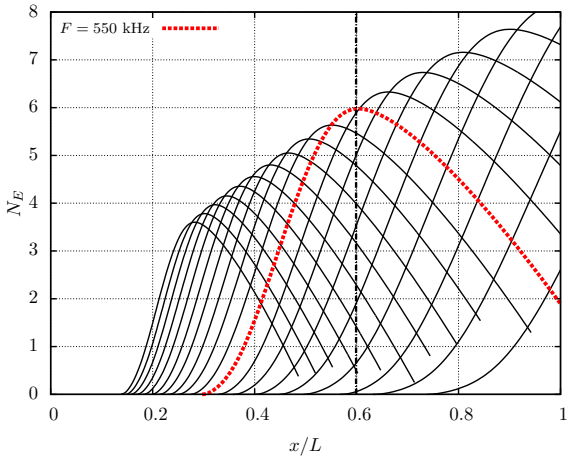

Figure 9. PSE predictions for N-factor based on energy norm E of planar second mode disturbances in an unperturbed Mach 6 circular cone boundary layer. The frequency is varied from $F = 350$ kHz to 800 kHz. The thick red dashed line denotes the frequency that first reaches $N_E = 6$ ($F = 550$ kHz). The vertical black dot-dashed line denotes the measured transition location.[48]

Here, we consider an initial disturbance location of $x_0/L = 0.2$ and a final location of $x_1/L = 0.4$. Figure 10(a) shows that the optimal azimuthal wavenumber that leads to a maximum energy gain, $G = E(x_1)/E(x_0)$, is found to be $m = 50$. For these parameters, the optimal energy gain in the limit of infinitesimal streak amplitudes is $G = 4,017$. The components of the initial and final optimal perturbations

are plotted in Figs. 10(b) and 10(c), respectively. The range $[x_0, x_1]$ has been chosen to obtain appreciable streak amplitudes over a majority of the cone length as shown in Fig. 11. As in the Mach 3 flat plate case, the streak amplitude parameter A corresponds to the maximum streak amplitude As_u achieved by a linear perturbation with the same initial amplitude, which is given by Eq. (12), with $E_{lin,A=1} = 6.01 \times 10^{-3}$ in the present case. The effect of nonlinearity on the streak evolution is very similar to that in the Mach 3 flat plate case, namely, a reduction of the streak amplitude relative to the linear prediction and an upstream displacement of the location corresponding to the maximum streak amplitude for each A.

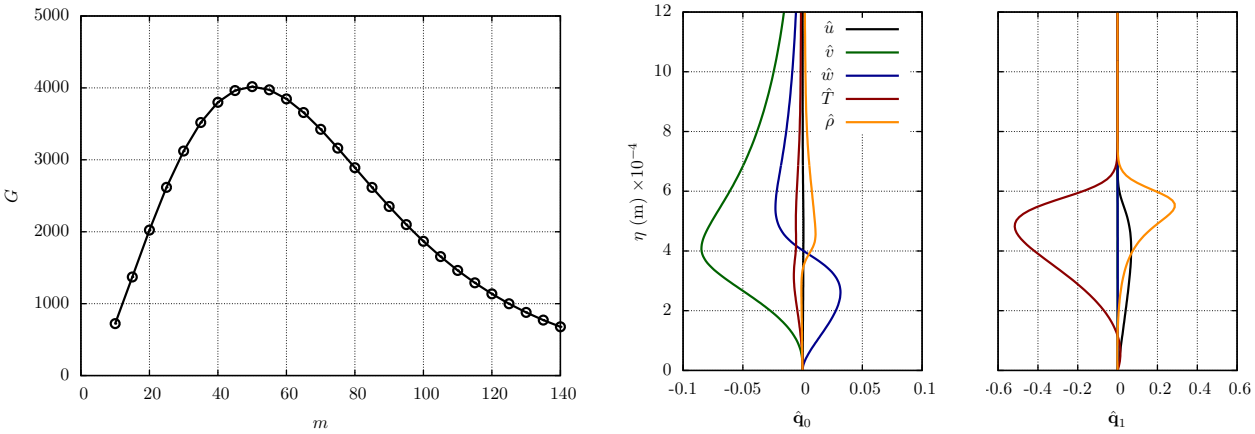

(a) Optimum energy gain (b) Initial perturbation (c) Final perturbation

Figure 10. Optimal energy gain in the Mach 6 circular cone boundary layer with initial and final disturbance locations at $x_0/L = 0.2$ and $x_1/L = 0.4$, respectively. Also, initial and final amplitude vectors with $m = 50$. The amplitude vectors are normalized with local energy norm $\hat{E}$ as defined in Eq. (6).

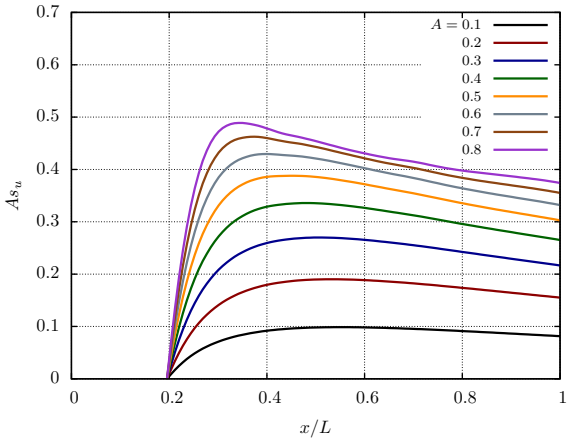

Figure 11. Evolution of streak amplitudes based on u, As_u, of finite-amplitude streaks initialized at the $x_0/L = 0.2$ with $m = 50$.

The PDE-based EVP analysis is used to obtain the growth rates of fundamental and subharmonic sinuous and varicose modes at $x/L = 0.5$ for the selected streak amplitudes from Fig. 11. Figure 12 shows the local growth rates as a function of disturbance frequency. For reference, the growth rates of the first mode instabilities for the unperturbed flow ($A = 0$), corresponding to the same wavenumber as the streak (FM_1), i.e., $m = 50$, and to one half of the streak wavenumber ($\mathrm{FM}_{1/2}$), i.e., $m = 25$, are also included in Figs. 12(a) and 12(b), respectively. The first mode is unstable for both $m = 25$ and $m = 50$ and the corresponding sinuous modes are observed to emerge from the first mode as the streak amplitude is increased from zero, this behavior being similar to that in the supersonic flat plate case. Again, the sinuous modes are more unstable than the varicose modes. The mode shapes of the S, V, SS, and SV modes are rather similar to those in Figs. 5 and 6 for the Mach 3 flat plate case. Therefore, the mode shapes for the present case are omitted from this section. Further results for a wider range of streak amplitudes and instability frequencies, including the effect of the finite-amplitude streaks on the second mode instability, can be found in Paredes et al.[32,49]

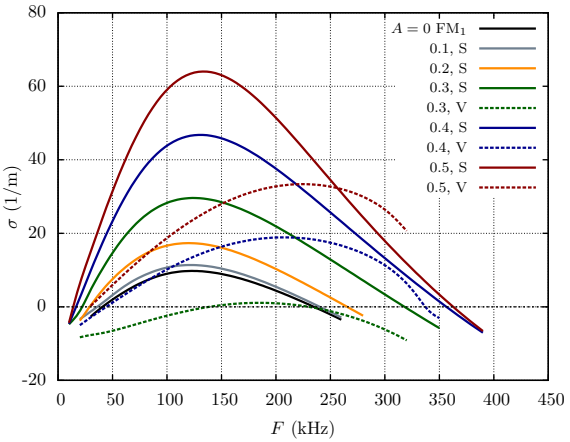

(a) Growth rate spectra of streak instabilities with fundamental azimuthal wavenumber

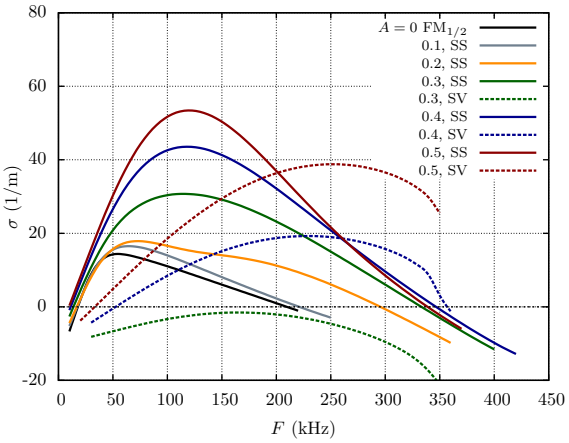

(b) Growth rate spectra of streak instabilities with subharmonic azimuthal wavenumber

Figure 12. Growth rates ($\sigma = -\alpha_i$) of (a) fundamental sinuous (S) and varicose (V) modes and (b) subharmonic sinuous (SS) and subharmonic varicose (SV) modes of finite-amplitude streaks initialized at $x/L = 0.2$ with $m = 50$, computed with PDE-based EVP. The analysis is performed at location $x/L = 0.5$.

N-factor calculations are presented next for the S and SS instability modes by using the linear form of the plane-marching PSE. As shown by Paredes et al.,[32] the N-factor curves corresponding to S and SS modes show a similar trend as that in Fig. 7 for the Mach 3 flat plate boundary layer. The S modes first become unstable at a streamwise position that is downstream of the streak initialization. On the other hand, the SS modes become unstable upstream of the initial streak location ($x_0/L = 0.2$). Therefore, they are initiated as first mode instabilities of the unperturbed boundary layer and then morph into the shear layer modes as the streak amplitude increases with x. The N-factor contours corresponding to S and SS modes in Fig. 13 are also in line with previous predictions for the Mach 3 flat plate case. In this case, the N-factor contours displayed in Fig. 13 correspond to $N_E = 6$, 10, and 14. For the purpose of discussion, the N-factor curve corresponding to $N_E = 6$ is assumed to represent the expected variation of transition onset location in a relatively noisy disturbance environment such as a conventional ground facility, whereas the curve $N_E = 10$ may be assumed to correspond to a quiet tunnel or a flight disturbance environment. The N-factor value of $N_E = 6$ is chosen as the noisy disturbance level, because as shown in Fig. 9 the measured transition location[48] corresponds to this value for the unperturbed boundary layer flow. The N-factor curves exhibit a similar trend to that observed in the Mach 3 case, with a large negative slope to begin with and then the slope decreases downstream. Again, the subharmonic instability mode reaches the N-factor threshold in a noisy disturbance environment at lower streak amplitudes, but the $N_E = 10$ threshold is first reached by the fundamental secondary instabilities. For the highest streak amplitude plotted in the figure, $A = 0.8$ ($As_{u,max} = 0.49$), the onset of transition in a low amplitude disturbance environment moves upstream to $x_{tr}/L = 0.42$ ($x_{tr}/x_{tr(As_u=0)} \approx 0.7$). The initial streak amplitude needed for bypass transition is $\hat{E}_0 > 7.5 \times 10^{-3}$, which corresponds to a streak amplitude parameter of approximately $A > 0.40$ ($As_{u,max} > 0.34$).

IV. Conclusions

This paper investigated a potential scenario for bypass transition via optimal transient growth in a supersonic, flat plate boundary layer at Mach 3 and in a hypersonic, 7° half-angle circular cone, boundary layer at Mach 6. The proposed transition mechanism involves modal versus transient amplification of secondary disturbance supported by the finite-amplitude streaks arising as a result of the transient growth. For both flows considered, the sinuous instability modes are found to be more amplified than varicose instability modes. While the mode shapes associated with streak instabilities are similar to those found in low-speed boundary layers, the present analysis shows that the nature of dominant streak instabilities can be rather different in high-speed boundary layers. To the best of our knowledge, the present set of results constitutes the first demonstration of subharmonic spanwise wavelengths of streaky motions in boundary layers flows being more strongly unstable than the streak instabilities with fundamental spanwise wavelengths. The subharmonic

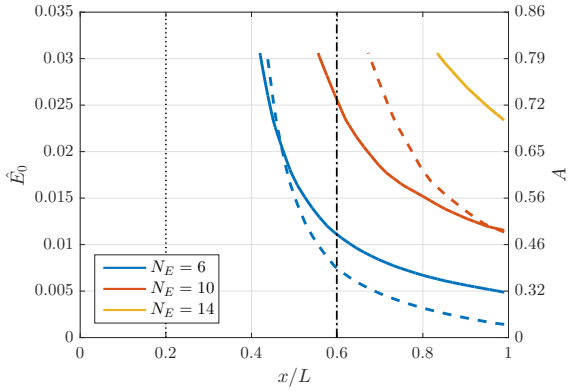

Figure 13. *N*-factor based on energy norm ($N_E = 6$, 10, and 14) of fundamental (solid lines) and subharmonic (dashed lines) sinuous, secondary instability modes on a Mach 6 circular cone boundary layer perturbed by optimal streaks with initial energy of $\hat{E}_0 = 1/L_\zeta\, E_0$ initiated at $x/L = 0.2$. The vertical dot-dashed line denotes the transition location based on $N_E = 6$ of planar second mode in the unperturbed flow.

modes control the onset of transition at smaller initial streak amplitudes, whereas the fundamental secondary modes take over beyond a threshold streak amplitude. The rather unique behavior of subharmonic mode amplification is shown to be related to the destabilizing influence of small amplitude streaks on oblique first mode disturbances, which tend to have longer spanwise wavelengths than those of the optimal stationary disturbances.

Acknowledgments

This work is supported by the NASA Transformational Tools & Technologies (TTT) project.

References

[1]Mack, L. M., "Boundary layer linear stability theory," *AGARD–R–709 Special course on stability and transition of laminar flow*, 1984, pp. 3.1–3.81.

[2]Schmid, P. and Henningson, D. S., *Stability and Transition in Shear Flows*, Springer, New York, 2001.

[3]Herbert, T., "Parabolized stability equations," *Ann. Rev. Fluid Mech.*, Vol. 29, 1997, pp. 245–283.

[4]Stuart, J., "The production on intense shear layers by vortex stretching and convection," NATO AGARD Report No. 514. (also: National Phys. Lab. Aeronaut. Res. Rep. 1147), 1965.

[5]Ellingsen, T. and Palm, E., "Stability of linear flow," *Phys. Fluids*, Vol. 18, No. 4, 1975, pp. 487–488.

[6]Landahl, M., "A note on algebraic instability of inviscid parallel shear flows," *J. Fluid Mech.*, Vol. 98, 1980, pp. 243–251.

[7]Butler, K. and Farrell, B., "Three-dimensional optimal perturbations in viscous shear flow," *Phys. Fluids*, Vol. 4, No. 8, 1992, pp. 1637–1650.

[8]Reddy, S. and Henningson, D., "Energy growth in viscous channel flow," *J. Fluid Mech.*, Vol. 252, 1993, pp. 209–238.

[9]Trefethen, L. N., Trefethen, A. E., Reddy, S. C., and Driscoll, T., "Hydrodynamic stability without eigenvalues," *Science*, Vol. 261, 1993, pp. 578–584.

[10]Hanifi, A., Schmid, P., and Henningson, D., "Transient growth in compressible boundary layer flow," *Phys. Fluids*, Vol. 8, 1996, pp. 51–65.

[11]Andersson, P., Berggren, M., and Henningson, D., "Optimal disturbances and bypass transition in boundary layers," *Phys. Fluids*, Vol. 11, 1999, pp. 134–150.

[12]Luchini, P., "Reynolds-number-independent instability of the boundary layer over a flat surface: Optimal perturbations," *J. Fluid Mech.*, Vol. 404, 2000, pp. 289–309.

[13]Tumin, A. and Reshotko, E., "Spatial theory of optimal disturbances in boundary layers," *Phys. Fluids*, Vol. 13, 2001, pp. 2097–2104.

[14]Tumin, A. and Reshotko, E., "Optimal disturbances in compressible boundary layers," *AIAA J.*, Vol. 41, 2003, pp. 2357–2363.

[15]Tumin, A. and Reshotko, E., "Optimal disturbances in the boundary layer over a sphere," AIAA Paper 2004-2241, 2004.

[16]Zuccher, S., Tumin, A., and Reshotko, E., "Parabolic approach to optimal perturbations in compressible boundary layers," *J. Fluid Mech.*, Vol. 556, 2006, pp. 189–216.

[17]Zuccher, S., Shalaev, I., Tumin, A., and Reshotko, E., "Optimal disturbances in the supersonic boundary layer past a sharp cone," *AIAA J.*, Vol. 45, 2007, pp. 366–373.

[18]Paredes, P., Choudhari, M., Li, F., and Chang, C., "Transient growth analysis of compressible boundary layers with parabolized stability equations," AIAA Paper (to appear), 2016.

[19]Paredes, P., Choudhari, M., Li, F., and Chang, C.-L., "Optimal growth in hypersonic boundary layers," *AIAA J.*, accepted, 2016.

[20]Reshotko, E., "Transient growth: A factor in bypass transition," *Phys. Fluids*, Vol. 13, 2001, pp. 1067–1075.

[21]Morkovin, M., Reshotko, E., and Herbert, T., "Transition in open flow systems - A reassessment," *Bull. Am. Phys. Soc.*, Vol. 39, 1994, pp. 1882.

[22]Reshotko, E., "Boundary layer transition, instability and control," AIAA Paper 94-0001, 1994.

[23]Reshotko, E. and Tumin, A., "Spatial theory of optimal disturbances in a circular pipe flow," *Phys. Fluids*, Vol. 13, 2001, pp. 991–996.

[24]Reshotko, E., "Preliminary experimental study of disturbances in a laminar boundary layer due to distributed surface roughness," AIAA Paper 81-1224, 1981.

[25]White, E., "Transient growth of stationary disturbances in a flat plate boundary layer," *Phys. Fluids*, Vol. 14, No. 12, 2002, pp. 4429–4439.

[26]Sharp, N. and White, E., "Roughness-induced transient growth on a hypersonic blunt cone," AIAA Paper 2014-0432, 2014.

[27]Murphy, J. and Rubesin, M., "Re-evaluation of heat-transfer data obtained in flight test of heat-sink shielded re-entry vehicles," *J. Spacecraft*, Vol. 3, No. 1, 1966, pp. 53–60.

[28]Reshotko, E. and Tumin, A., "The blunt body paradox - A case for transient growth," *Proc. of the IUTAM Laminar-Turbulent Symposium V*, edited by H. Fasel and W. Saric, Sedona, AZ, USA, 2000, pp. 403–408.

[29]Schneider, S., "Hypersonic boundary-layer transition on blunt bodies with roughness," AIAA Paper 2008-0501, 2008.

[30]Theiss, A., Hein, S., Heitmann, D., Ali, S., and Radespiel, R., "Numerical and experimental investigation of laminar-turbulent boundary layer transition on a blunt generic re-entry capsule," AIAA Paper 2014-2353, 2014.

[31]Paredes, P., Choudhari, M., and Li, F., "Bypass transition in a supersonic flat plate boundary layer," *Phys. Rev. Fluids*, submitted, 2016.

[32]Paredes, P., Choudhari, M., and Li, F., "Effect of nonlinear transient growth on hypersonic boundary layer transtion," *J. Fluid Mech.*, to be submitted, 2016.

[33]Pralits, J., Airiau, C., Hanifi, A., and Henningson, D., "Sensitivity analysis using adjoint parabolized stability equations for compressible flows," *Flow Turbul. Combust.*, Vol. 65, 2000, pp. 183–210.

[34]Tempelmann, D., Hanifi, A., and Henningson, D., "Spatial optimal growth in three-dimensoinal boundary layers," *J. Fluid Mech.*, Vol. 646, 2010, pp. 5–37.

[35]Tempelmann, D., Hanifi, A., and Henningson, D., "Spatial optimal growth in three-dimensoinal compressible boundary layers," *J. Fluid Mech.*, Vol. 704, 2012, pp. 251–279.

[36]Li, F. and Malik, M., "Mathematical nature of parabolized stability equations," *R. Kobayashi (Ed.), Laminar-Turbulent Transition, Springer*, 1994, pp. 205–212.

[37]Li, F. and Malik, M., "On the nature of the PSE approximation," *Theor. Comp. Fluid Dyn.*, Vol. 8, 1996, pp. 253–273.

[38]Li, F. and Malik, M., "Spectral analysis of parabolized stability equations," *Compt. Fluids*, Vol. 26, No. 3, 1997, pp. 279–297.

[39]Haj-Hariri, H., "Characteristics analysis of the parabolized stability equations," *Stud. Appl. Math.*, Vol. 92, 1994, pp. 41–53.

[40]Andersson, P., Henningson, D., and Hanifi, A., "On a stabilization procedure for the parabolic stability equations," *J. Engng. Math.*, Vol. 33, 1998, pp. 311–332.

[41]Bagheri, S. and Hanifi, A., "The stabilizing effect of streaks on Tollmien-Schlichting and oblique waves: a parametric study," *Phys. Fluids*, Vol. 19, 2007, pp. 078103–1–078103–4.

[42]Mack, L. M., "Boundary Layer Stability Theory," Tech. Rep. JPL Rept. 900-277, California Institute of Technology, Pasadena, CA, 1969.

[43]Paredes, P., *Advances in global instability computations: from incompressible to hypersonic flow*, Ph.D. thesis, Universidad Politécnica de Madrid, 2014.

[44]Paredes, P., Hanifi, A., Theofilis, V., and Henningson, D., "The nonlinear PSE-3D concept for transition prediction in flows with a single slowly-varying spatial direction," *Procedia IUTAM*, Vol. 14C, 2015, pp. 35–44.

[45]Andersson, P., Brandt, L., Bottaro, A., and Henningson, D., "On the breakdown of boundary layer streaks," *J. Fluid Mech.*, Vol. 428, 2001, pp. 29–60.

[46]Martín, J. and Martel, C., "Nonlinear streak computation using boundary region equations," *Fluid Dyn. Res.*, Vol. 44, 2012, pp. 045503.

[47]Paredes, P., Choudhari, M., and Li, F., "Interaction of supersonic boundary layer instabilities with stationary streamwise streaks," XXIV ICTAM, 21-26 August 2016, Montreal, Canada, submitted, 2016.

[48]Grossir, G., Musutti, D., and Chazot, O., "Flow characterization and boundary layer transition studies in VKI hypersonic facilities," AIAA Paper 2015-0578, 2015.

[49]Paredes, P., Choudhari, M., and Li, F., "Transition delay in hypersonic boundary layers via optimal perturbations," *Phys. Rev. Let.*, submitted, 2016.